Partonic mean-field effects on matter and antimatter elliptic flows

Taesoo Song,[1,*] Salvatore Plumari,[2,†] Vincenzo Greco,[2,‡] Che Ming Ko,[3,§] and Feng Li[1,¶]

[1] *Cyclotron Institute and Department of Physics and Astronomy, Texas A&M University, College Station, TX*
[2] *Dipartimento di Fisica e Astronomia, Universit di Catania, Via S. Sofia 64, 95125 Catania, Italy*
[3] *Cyclotron Institute and Department of Physics and Astronomy, Texas A&M University, College Station, TX 77843-3366, USA*

Using a partonic transport model based on the Nambu-Jona-Lasinio (NJL) model, we study the effect of scalar and vector mean fields on the elliptic flows of quarks and antiquarks in relativistic heavy ion collisions in Au+Au collisions at $\sqrt{s_{\rm NN}} = 7.7$ GeV and impact parameter $b = 8$ fm that leads to the production of a baryon-rich matter. Converting quarks and antiquarks at hadronization to hadrons via the quark coalescence model, we further study the dependence of the transverse momentum integrated relative elliptic flow differences between protons and antiprotons, lambda and anti-lambdas, and positively and negatively charged kaons on the strength of the quark vector coupling. Our results suggest that a relative weak vector coupling seems to be needed to describe the experimental data measured by the STAR Collaboration in the Beam Energy Scan (BES) program at the Relativistic Heavy Ion Collider (RHIC).

PACS numbers: 25.75.Nq, 25.75.Ld

I. INTRODUCTION

In relativistic heavy-ion collisions, a hot and dense matter that consists of deconfined quarks and gluons is produced in the initial stage. Depending on the energy of collisions, this so-called quark-gluon plasma (QGP) can have various temperatures and baryon chemical potentials. As the formed QGP expands and cools, it is converted to the normal hadronic matter (HM). Therefore, heavy ion collisions at relativistic energies provide the possibility to study the phase structure of the strongly interacting matter that is described by the quantum chromodynamics (QCD). For the top energy available at RHIC and at the Large Hadron Collider (LHC), the produced QGP are nearly baryon free and thus has very small baryon chemical potentials. According to the lattice QCD calculations [1, 2], the transition from the QGP phase to the HM phase in this region of the phase diagram is a smooth crossover without a clear phase boundary. The phase transition between QGP and HM is, however, expected to change from the crossover to a first-order transition at certain finite baryon chemical potential called the critical point in the QCD phase diagram [3–6]. To probe this region of the QCD phase diagram, the beam energy scan (BES) program at much lower energies of $\sqrt{s_{\rm NN}} = 7.7$, 11.5, and 39 GeV than the top energy have recently been carried out at RHIC by the STAR Collaboration [7]. Although no definitive signals for a first-order phase transition and the critical end point have been established, a number of interesting results have been observed [8]. One of them is the increasing difference between the elliptic flows of particles and antiparticles, thus a breaking of the number of constituent quark number scaling of elliptic flows, as the collision energy decreases. Such a behavior cannot be described by a simple hydrodynamic or hadronic cascade model even if the quark coalescence is considered during the hadronization of produced QGP [9]. Several theoretical attempts have been made to explain this surprising experimental result [10–13]. In particular, the effect of hadronic mean-field potentials on the elliptic flows of particles and antiparticles has been studied in Ref. [12] using a multiphase transport (AMPT) model that includes both initial partonic and final hadronic scatterings [14, 15]. Because of the different mean-field potentials for particles and antiparticles in the baryon-rich matter formed in these collisions, p, K^+ and π^- were found to have larger elliptic flows than $\bar{p}$, K^- and π^+, respectively, as observed in experiments. However, these results are not in quantitative agreement with the experimental data. The calculated relative integrated elliptic flow difference between particles and antiparticles, defined by $[v_2(\text{particle}) - v_2(\text{antiparticle})]/v_2(\text{particle})$, for Au+Au collisions at $\sqrt{s_{\rm NN}} = 7.7$ GeV and impact parameter $b = 8$ fm is about a factor of two smaller than the measured values of 63 % for p and $\bar{p}$ and -3 % for π^+ and π^- but is about a factor two larger than the measured value of 13 % for K^+ and K^-.

The study in Ref. [12] has neglected the effect of mean-field potentials in the initial partonic stage. As shown in Ref. [16] using a partonic transport model based on the NJL model for Au+Au collisions at $\sqrt{s_{\rm NN}} = 200$ GeV, where the baryon chemical potential of produced matter is small, the attractive scalar mean field on quarks and antiquarks was found to reduce their elliptic flows. In the present study, we extend the study of Ref. [16] to also include the effect due to the vector mean field in the quark matter. Since the latter is repulsive for quarks

*Electronic address: songtsoo@yonsei.ac.kr
†Electronic address: salvatore.plumari@hotmail.it
‡Electronic address: greco@lns.infn.it
§Electronic address: ko@comp.tamu.edu
¶Electronic address: fengphysics@gmail.edu

and attractive for antiquarks in baryon-rich quark matter, it increases the elliptic flow of quarks and reduces that of antiquarks. Using the coalescence model to convert quarks and antiquarks to hadrons at hadronization, we further show that the vector mean field in the QGP also leads to an increase of the elliptic flows of p, Λ, and K^- and a decrease of the elliptic flows of $\bar{p}$, $\bar{\Lambda}$, and K^+. Our results thus help to explain the large p and $\bar{p}$ but small K^+ and K^- relative v_2 differences observed in experiments. Also, information on the strength of the quark vector mean field is important for understanding the equation of state of QGP at finite baryon chemical potential, which at present cannot reliably be obtained from lattice studies. As shown in studies based on both the NJL and the Polyakov-Nambu-Jona-Lasinio (PNJL) models [3–6], the existence and the location of the critical point in the QCD phase diagram is sensitive to the strength of isoscalar vector coupling. A critical point only exists if the strength of the vector coupling is small. Otherwise, the phase transition is always a crossover.

This paper is organized as follows: In Sec. II, we briefly review the NJL model for three flavors of quarks and antiquarks and discuss the mean-field approximations. We then describe in Sec. III the partonic transport model, with the mean fields taken from the NJL model, that is used to study the time evolution of the parton phase-space distributions in relativistic heavy-ion collisions. Results on the quark and antiquark elliptic flows from solving the transport model are shown in Sec. IV together with those of p and $\bar{p}$, Λ and $\bar{\Lambda}$, and K^+ and K^- that are obtained from quarks and antiquarks by using the coalescence model at hadronization. Finally, a summary is given in Sec. V.

II. THE NAMBU-JONA-LASINIO MODEL

The NJL Lagrangian for three quark flavors has the form [6]:

$$\begin{aligned}\mathcal{L} &= \bar{\psi}(i\not{\partial} - M)\psi + \frac{G}{2}\sum_{a=0}^{8}\left[(\bar{\psi}\lambda^a\psi)^2 + (\bar{\psi}i\gamma_5\lambda^a\psi)^2\right] \\ &+ \sum_{a=0}^{8}\left[\frac{G_V}{2}(\bar{\psi}\gamma_\mu\lambda^a\psi)^2 + \frac{G_A}{2}(\bar{\psi}\gamma_\mu\gamma_5\lambda^a\psi)^2\right] \\ &- K\left[\det{}_f\left(\bar{\psi}(1+\gamma_5)\psi\right) + \det{}_f\left(\bar{\psi}(1-\gamma_5)\psi\right)\right], \quad (1)\end{aligned}$$

where $\psi = (\psi_u, \psi_d, \psi_s)^T$, $M = \mathrm{diag}(m_u, m_d, m_s)$ and λ^a is the Gell-Mann matrices with λ^0 being identity matrix multiplied by $\sqrt{2/3}$. In the case that the vector and axial-vector interactions are generated by the Fierz transformation of the scalar and pseudo-scalar interactions, their coupling strengths are given by $G_V = G_A = G/2$. The last term is the Kobayashi-Maskawa-t'Hooft (KMT) interaction that breaks $U(1)_A$ symmetry [17] with $\det_f$ denoting the determinant in flavor space [18]:

$$\det{}_f(\bar{\psi}\Gamma\psi) = \sum_{i,j,k}\varepsilon_{ijk}(\bar{u}\Gamma q_i)(\bar{d}\Gamma q_j)(\bar{s}\Gamma q_k). \quad (2)$$

It gives rise to four-point interactions in two flavors and six-point interactions in three flavors. In the two flavor case, the sum of scalar and pseudo-scalar interactions and the KMT interaction with K=-G reduces to the original NJL model [3, 19].

Considering only the flavor singlet vector interaction in the second interaction term and taking the mean-field approximation, the Lagrangian becomes [3, 20]

$$\mathcal{L} = \bar{\psi}\left(i\partial^\mu - \frac{2}{3}G_V\langle\bar{\psi}\gamma^\mu\psi\rangle\right)\gamma_\mu\psi - \bar{\psi}M^*\psi + ... \quad (3)$$

where $M^* = \mathrm{diag}(M_u, M_d, M_s)$ with

$$\begin{aligned}M_u &= m_u - 2G\langle\bar{u}u\rangle + 2K\langle\bar{d}d\rangle\langle\bar{s}s\rangle, \\ M_d &= m_d - 2G\langle\bar{d}d\rangle + 2K\langle\bar{s}s\rangle\langle\bar{u}u\rangle, \\ M_s &= m_s - 2G\langle\bar{s}s\rangle + 2K\langle\bar{u}u\rangle\langle\bar{d}d\rangle, \quad (4)\end{aligned}$$

and ... denotes constant terms such as $\langle\bar{\psi}\psi\rangle^2$. The mean fields are calculated as following:

$$\begin{aligned}\langle\bar{q}_i q_i\rangle &= -2M_i N_c\int\frac{d^3\mathbf{k}}{(2\pi)^3 E_i}\,[1 - f_i(k) - \bar{f}_i(k)], \\ \langle\bar{\psi}\gamma^\mu\psi\rangle &= 2N_c\sum_{i=u,d,s}\int\frac{d^3\mathbf{k}}{(2\pi)^3 E_i}\,k^\mu[f_i(k) - \bar{f}_i(k)], \quad (5)\end{aligned}$$

where N_c is the number of colors, and $f_i(k)$ and $\bar{f}_i(k)$ are number densities of flavor i and its anti-flavor, respectively. Because the NJL model is not renormalizable, the momentum integration requires a cut-off Λ. For the parameters in the NJL model, we use those from Refs. [6, 21], that is, $m_u = m_d = 3.6$ MeV, $m_s = 87$ MeV, $G\Lambda^2 = 3.6$, $K\Lambda^2 = 8.9$, and $\Lambda = 750$ MeV, unless otherwise stated.

III. TRANSPORT EQUATION FOR PARTONIC MATTER

Similar to that for the hadronic matter [23, 24], the time evolution of the partonic matter produced in relativistic heavy ions collisions can be described by the following transport equation for the partonic phase-space distribution function $f(\mathbf{x}, \mathbf{p})$;

$$\frac{\partial}{\partial t}f + \vec{v}\cdot\nabla_x f - \nabla_x H\cdot\nabla_p f = \mathcal{C}, \quad (6)$$

where $H(\mathbf{x}, \mathbf{p})$ is the hamiltonian of a quark in the self-consistent scalar and vector mean fields and $\mathcal{C}$ denotes the collision term that describes the parton scattering, for which we use a constant cross section of 10 mb.

For a parton in the scalar and vector mean fields derived from the NJL model, we have

$$H = \sqrt{M^{*2} + p^{*2}} \pm g_V \rho^0 \equiv E^* \pm g_V \rho^0, \tag{7}$$

where $\mathbf{p}^* = \mathbf{p} \mp g_V \boldsymbol{\rho}$ with $\boldsymbol{\rho} \equiv \langle \bar{\psi} \boldsymbol{\gamma} \psi \rangle$ and $g_V \equiv (2/3) G_V$; $\rho^0 \equiv \langle \bar{\psi} \gamma^0 \psi \rangle$ being the net baryon density, and the upper and lower signs are for quarks and antiquarks, respectively.

In the test particle method of solving the transport equation [25], their equations of motion are given by

$$\frac{dx_i}{dt} = \frac{\partial H}{\partial p_i} = \frac{p_i^*}{E^*}, \tag{8}$$

$$\frac{dp_i}{dt} = -\frac{\partial H}{\partial x_i} = -\frac{M^*}{E^*}\frac{\partial M^*}{\partial x_i} + g_V \left(v_j \frac{\partial \rho_j}{\partial x_i} - \frac{\partial \rho_0}{\partial x_i} \right). \tag{9}$$

We note that in the case that the effective mass of the (anti)quark does not change with position, the LHS of Eq. (9) leads to the following Lorentz force:

$$F_i = \frac{dp_i^*}{dt} = \frac{dp_i}{dt} - g_V \frac{\rho_i}{dt} = g_V \left(v_j \frac{\partial \rho_j}{\partial x_i} - \frac{\partial \rho_0}{\partial x_i} - \frac{d\rho_i}{dt} \right) = g_V (\mathbf{v} \times \mathbf{B} + \mathbf{E})_i, \tag{10}$$

with $\mathbf{B} = \nabla \times \boldsymbol{\rho}$ and $\mathbf{E} = -\nabla \rho^0 - \partial \boldsymbol{\rho} / \partial t$.

IV. RESULTS

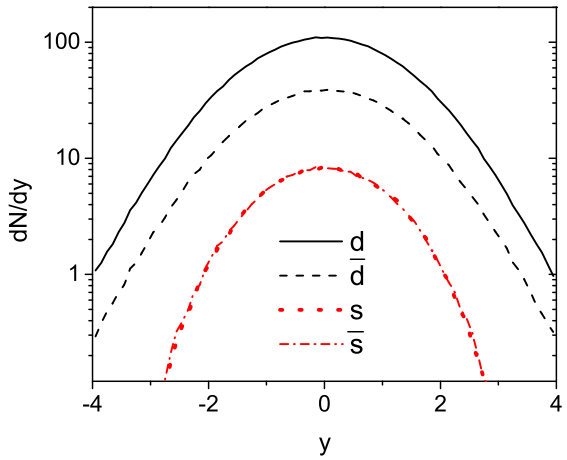

FIG. 1: (Color online) Rapidity distributions of down and strange quarks and their antiquarks in Au+Au collisions at $\sqrt{s_{\rm NN}} = 7.7$ GeV and impact parameter $b = 8$ fm from the AMPT model.

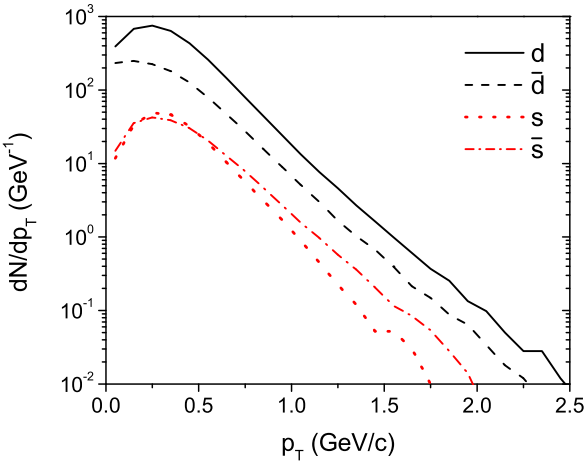

FIG. 2: (Color online) Transverse momentum distributions of down and strange quarks and their antiquarks in Au+Au collisions at $\sqrt{s_{\rm NN}} = 7.7$ GeV and impact parameter $b = 8$ fm from the AMPT model.

For the initial quark and antiquark rapidity and transverse momentum distributions in a relativistic heavy-ion collision, we use the valence quarks and antiquarks converted from hadrons that are obtained from the Heavy-Ion Jet Interaction Generator (HIJING) model [22] through Lund string fragmentation as implemented in the AMPT model with string melting [15]. They are given in Fig. 1 and Fig. 2 for down and strange quarks and their antiquarks in Au+Au collisions at $\sqrt{s_{\rm NN}} = 7.7$ GeV and at impact parameter $b = 8$ fm. The distributions of up and anti-up quarks are slightly smaller than those of down and anti-down quarks. It shows that the number of down quarks is more than twice that of anti-down quarks in heavy ion collisions at this energy, indicating that the produced quark matter is baryon-rich. We note that strange quarks have a softer transverse momentum spectrum than anti-strange quarks because they are mostly from the conversion of hyperons while anti-strange quarks are mostly from the conversion of strange mesons.

We solve Eqs. (5), (8), and (9) numerically and then use the resulting parton momentum distributions to evaluate their elliptic flow v_2 according to

$$v_2 = \frac{1}{N} \sum_{i=1}^{N} \frac{(p_x^{*2})_i - (p_y^{*2})_i}{(p_x^{*2})_i + (p_y^{*2})_i}, \tag{11}$$

where N is the total number of test particles.

A. quark and antiquark elliptic flows

Figure 3 shows the integrated v_2 of light and strange quarks and antiquarks as functions of time for the cases

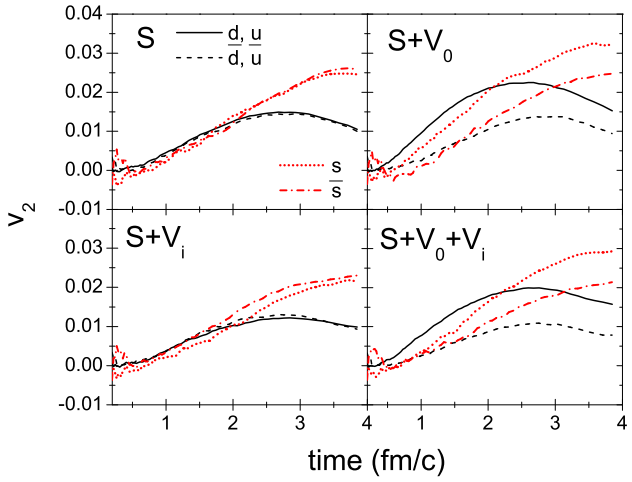

FIG. 3: (Color online) Integrated elliptic flow v_2 of light and strange quarks and antiquarks at mid-rapidity ($|y| < 1$) as functions of time in Au+Au collisions at $\sqrt{s_{\rm NN}} = 7.7$ GeV and at impact parameter $b = 8$ fm for the cases of including only scalar mean field (S), scalar and time component of vector mean field ($S + V_0$), scalar and space component of vector mean field ($S+V_i$), and scalar and both components of vector mean field ($S + V_0 + V_i$)

of including only scalar mean field, scalar and time component of vector mean field, scalar and space component of vector mean field, and scalar and both components of vector mean field. It is seen that the quark and antiquark v_2 are essentially the same if only the scalar mean field is included in determining their propagations in the quark matter. This is due to the fact that through ∇M^* in Eq. (9) the scalar mean field generates the same attractive force on quarks and antiquarks. Including the time component of vector mean field caused by excess quarks leads to a larger quark than antiquark v_2 due to the resulting repulsive force on quarks and attractive force on antiquarks. We note that v_2 is generated by the gradient of the pressure, which always points outward in heavy-ion collisions but is enhanced by a repulsive force and reduced by an attractive force. Therefore, the time-component of vector mean field enhances the v_2 of quarks and suppresses that of antiquarks while the attractive scalar mean field suppresses both quark and antiquark v_2 [16]. As to the space component of vector mean field, its effect on the v_2 of quarks and antiquarks is opposite to that from the time component but with a much smaller magnitude. The other difference between the effect of space component and that of time component of vector mean field is that the splitting between v_2 of quarks and antiquarks starts earlier in the time-component case than in the space-component case. The reason is that the space component of vector mean field is proportional to the baryon current that takes time to develop and is not large unless the relativistic flow streams are large [26]. The net result of the partonic mean fields in our study is that it leads to a larger quark than antiquark v_2 if the produced quark matter is baryon-rich. These behaviors are seen for both light and strange quarks. On the other hand, while the integrated v_2 of strange quarks continues to increase with time, that of light quarks decreases at later times. This is due to the stronger attractive scalar mean field for light quarks than for strange quarks as a result of the larger decrease of the light quark condensate along the radial direction than that of the strange condensate and the smaller light quark mass than the strange quark mass.

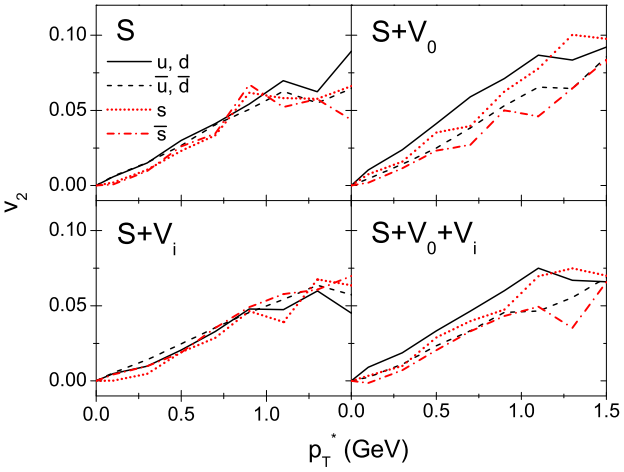

FIG. 4: (Color online) Elliptic flow v_2 of light and strange quarks and antiquarks at mid-rapidity ($|y| < 1$) as functions of transverse momentum at hadronization for the cases of including only scalar mean field (S), scalar and time component vector mean-field ($S+V_0$), scalar and space component vector mean field ($S+V_i$), and scalar and both components of vector mean-field ($S + V_0 + V_i$)

For the transverse momentum dependence of quark and antiquark v_2, they are shown in Fig. 4 for those at the end of the partonic phase, which is about 2.1 fm/c after the start of the partonic evolution when the energy density in the center of produced quark matter decreases to 0.8 GeV/fm^3, again for the cases of including only scalar mean field, scalar and time component of vector mean field, scalar and space component of vector mean field, and scalar and both components of vector mean field. For the last case, the difference between the integrated v_2 of up and down quarks and their antiquarks is about 49 % of the integrated v_2 of up and down quarks, and that between strange quarks and anti-strange quarks is about 34 % of the integrated v_2 of strange quarks.

B. hadron elliptic flows

To study how different quark and antiquark v_2 is reflected in the v_2 of produced hadrons, we use the coa-

lescence model to convert them to hadrons at hadronization. In this model, the probability for a quark and an antiquark to form a meson is proportional to the quark Wigner function of the meson with the proportional constant given by the statistical factor g_M for colored spin-1/2 quark and antiquark to form a colorless meson [27–29], that is

$$f_M(\boldsymbol{\rho}, \mathbf{k}_\rho) = 8 g_M \exp\left[-\frac{\boldsymbol{\rho}^2}{\sigma_\rho^2} - \mathbf{k}_\rho^2 \sigma_\rho^2\right], \tag{12}$$

where

$$\boldsymbol{\rho} = \frac{1}{\sqrt{2}}(\mathbf{r}_1 - \mathbf{r}_2), \quad \mathbf{k}_\rho = \sqrt{2}\,\frac{m_2\mathbf{k}_1 - m_1\mathbf{k}_2}{m_1+m_2}, \tag{13}$$

with m_i, $\mathbf{r}_i$ and $\mathbf{k}_i$ being the mass, position and momentum of quark (antiquark) i, respectively. The width parameter σ_ρ in the Wigner function is related to the root-mean-square radius of the meson via

$$\begin{aligned}\langle r_M^2\rangle &= \frac{3}{2}\frac{m_1^2+m_2^2}{(m_1+m_2)^2}\sigma_\rho^2 \\ &= \frac{3}{8}\frac{m_1^2+m_2^2}{\omega m_1 m_2 (m_1+m_2)},\end{aligned} \tag{14}$$

where the second line follows if we use the relation $\sigma_\rho = 1/\sqrt{\mu_1\omega}$ in terms of the oscillator frequency ω and the reduced mass $\mu_1 = 2(1/m_1 + 1/m_2)^{-1}$.

The probability for three quarks or antiquarks to coalescence to a baryon or an anti-baryon is similarly proportional to the quark Wigner function of the baryon, i.e.,

$$\begin{aligned}&f_B(\boldsymbol{\rho}, \boldsymbol{\lambda}, \mathbf{k}_\rho, \mathbf{k}_\lambda) \\ &= 8^2 g_B \exp\left[-\frac{\boldsymbol{\rho}^2}{\sigma_\rho^2} - \frac{\boldsymbol{\lambda}^2}{\sigma_\lambda^2} - \mathbf{k}_\rho^2\sigma_\rho^2 - \mathbf{k}_\lambda^2\sigma_\lambda^2\right],\end{aligned} \tag{15}$$

where g_B is the statistical factor for three colored spin-1/2 quarks to form a colorless baryon, and

$$\begin{aligned}\boldsymbol{\lambda} &= \sqrt{\frac{2}{3}}\left(\frac{m_1\mathbf{r}_1 + m_2\mathbf{r}_2}{m_1+m_2} - \mathbf{r}_3\right), \\ \mathbf{k}_\lambda &= \sqrt{\frac{3}{2}}\,\frac{m_3(\mathbf{k}_1+\mathbf{k}_2) - (m_1+m_2)\mathbf{k}_3}{m_1+m_2+m_3}.\end{aligned} \tag{16}$$

The width parameter σ_λ is related to the oscillator frequency by $(\mu_2\omega)^{-1}$, with $\mu_2 = (3/2)[1/(m_1+m_2) + 1/m_3]^{-1}$. The root-mean-square radius of a baryon or an antibaryon is then given by

$$\begin{aligned}&\langle r_B^2\rangle \\ &= \frac{1}{2}\frac{m_1^2(m_2+m_3) + m_2^2(m_3+m_1) + m_3^2(m_1+m_2)}{\omega(m_1+m_2+m_3)m_1m_2m_3}.\end{aligned} \tag{17}$$

For the mesons K^+ and K^-, the baryons p and Λ, and the anti-baryons $\bar{p}$ and $\bar{\Lambda}$ considered here, their statistical factors in the quark coalescence are $g_{K^+} = g_{K^-} = 1/36$ and $g_p = g_\Lambda = g_{\bar{p}} = g_{\bar{\Lambda}} = 1/108$. The oscillator frequency ω is determined from the root-mean-square radius of the produced hadron, which is taken to be 0.6 fm for K^+ and K^-, and 0.877 fm [30] for both p and Λ as well as for $\bar{p}$ and $\bar{\Lambda}$. We do not consider π^+ and π^- elliptic flows because they are affected similarly by the partonic mean fields as a result of similar elliptic flows for u and d quarks as well for $\bar{u}$ and $\bar{d}$ antiquarks.

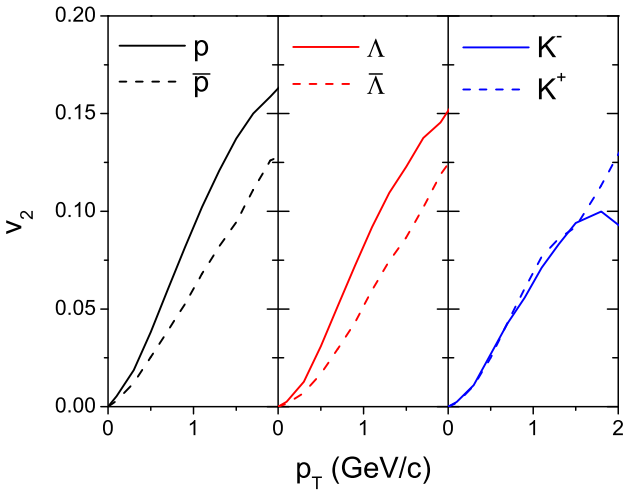

FIG. 5: (Color online) Elliptic flows v_2 of midrapidity ($|y| < 1$) p and $\bar{p}$ (left panel), Λ and $\bar{\Lambda}$ (middle panel), and K^+ and K^- (right panel) at hadronization as functions of transverse momentum.

Figure 5 shows the v_2 of p and $\bar{p}$ (left panel), Λ and $\bar{\Lambda}$ (middle panel), and K^+ and K^- (right panel), at hadronization as functions of transverse momentum. It is seen that the quark coalescence leads to a larger hadron v_2 than the quark v_2 at same transverse momentum. Furthermore, the v_2 of p, Λ, and K^- are respectively larger than those of $\bar{p}$, $\bar{\Lambda}$, and K^+, leading to the relative differences between their integrated v_2, $[v_2(\text{particle}) - v_2(\text{antiparticle})]/v_2(\text{particle})$, of 36.5, 44.3, and -5.0 % respectively, compared with the values 63±14, 54±27, and 13±2 % measured in experiments.

The dependence of the relative difference between integrated particle and antiparticle v_2 on the vector coupling g_V is shown in Fig. 6. Besides the value $g_V/G = 0.33$, which is from the Fierz transformation, two other values of 0.165 and 0.73, the latter from Ref. [21], are also used. The relative integrated v_2 differences are seen to increase almost linearly with the strength of the vector coupling but become saturated beyond the value $g_V/G = 0.33$.

V. SUMMARY

We have studied the effect of partonic mean fields on the elliptic flows of quarks and antiquarks in a brayon-rich quark matter by using a transport model based on

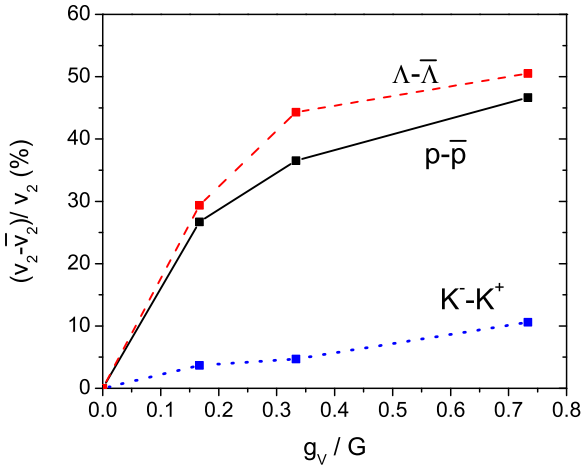

FIG. 6: (Color online) Relative differences between integrated v_2 of mid-rapidity ($|y| < 1$) p and $\bar{p}$, Λ and $\bar{\Lambda}$, and K^- and K^+ at hadronization for several values of the isoscalar vector coupling.

the NJL model. For the scalar mean field, which is attractive for both quarks and antiquarks, it leads to a similar reduction of the quark and antiquark v_2 as first found in Ref. [16]. The vector mean field, on the other hand, has very different effects on quarks and antiquarks in the baryon-rich matter as it is repulsive for quarks and attractive for antiquarks. The time component of vector mean field turns out to have the strongest effect, resulting in a significant splitting of the quark and antiquark v_2 as a result of enhanced quark v_2 and suppressed antiquark v_2. The space component of vector mean field has, however, an opposite effect; it suppresses v_2 of quarks and enhances that of antiquark, although relatively small and appearing later in the partonic stage compared to that of the time component of vector mean field.

Using the quark coalescence model, we have further studied the elliptic flows of p, Λ, and K^+ and their antiparticles produced from the baryon-rich quark matter and found that the differences between particle and antiparticle elliptic flows are appreciable as a result of the different quark and antiquark v_2. The magnitude of the relative integrated v_2 difference between particles and their antiparticles depends on the strength of the vector coupling. For the one obtained from the Fierz transformation of the scalar interaction in the NJL model (g_v/G=0.33), the v_2 differences between p and $\bar{p}$, Λ and $\bar{\Lambda}$, and K^+ and K^-, are about 36.5, 44.3, and -5.0 %, respectively. Compared to the data from the BES experiments at RHIC, the calculated value for the relative v_2 difference is about a factor of two smaller for p and $\bar{p}$, slightly smaller for Λ and $\bar{\Lambda}$, and about a factor of two smaller but with an opposite sign for K^+ and K^-. Since hadronic mean fields can further increase the relative v_2 differences between p and $\bar{p}$, Λ and $\bar{\Lambda}$, and K^+ and K^- [12], a smaller vector coupling in the baryon-rich quark matter seems to be needed. Also, allowing chemical reactions of partons such as pair creation and annihilation of quark and antiquark is also expected to lead to a splitting of the quark and antiquark v_2 as shown in a recent study based on the ideal hydro+UrQMD hybrid model [13], which assumes local thermal and baryon chemical equilibrium in the initial stage of heavy ion collisions. A more quantitative study that includes both the partonic and hadronic mean-field effects as well as the chemical reactions in the partonic phase is needed before a definitive determination of the strength of vector interactions in the baryon-rich QGP can be achieved. Nevertheless, the upper bound inferred from the present study for the value of the vector coupling already has an important implication that a critical point is likely to exist in the QCD phase diagram based on the NJL model.

Acknowledgements

This work was supported in part by the U.S. National Science Foundation under Grant No. PHY-1068572, the Welch Foundation under Grant No. A-1358, and the ERC-StG under the Grant QGPDyn No. 259684.

[1] C. Bernard *et al.* [MILC Collaboration], Phys. Rev. D **71**, 034504 (2005).
[2] A. Bazavov, T. Bhattacharya, M. Cheng, C. DeTar, H. T. Ding, S. Gottlieb, R. Gupta and P. Hegde *et al.*, Phys. Rev. D **85**, 054503 (2012).
[3] M. Asakawa and K. Yazaki, Nucl. Phys. A **504**, 668 (1989).
[4] K. Fukushima, Phys. Rev. D **77**, 114028 (2008) [Erratum-ibid. D **78**, 039902 (2008)].
[5] S. Carignano, D. Nickel and M. Buballa, Phys. Rev. D **82**, 054009 (2010).
[6] N. M. Bratovic, T. Hatsuda and W. Weise, arXiv:1204.3788 [hep-ph].
[7] L. Kumar [STAR Collaboration], J. Phys. G G **38**, 124145 (2011).
[8] B. Mohanty [STAR Collaboration], J. Phys. G G **38**, 124023 (2011).
[9] V. Greco, M. Mitrovski and G. Torrieri, Phys. Rev. C **86** (2012) 044905
[10] J. C. Dunlop, M. A. Lisa and P. Sorensen, Phys. Rev. C **84**, 044914 (2011).
[11] Y. Burnier, D. E. Kharzeev, J. Liao and H. -U. Yee, Phys. Rev. Lett. **107**, 052303 (2011).
[12] J. Xu, L. -W. Chen, C. M. Ko and Z. -W. Lin, Phys. Rev. C **85**, 041901 (2012).
[13] J. Steinheimer, V. Koch and M. Bleicher,

arXiv:1207.2791 [nucl-th].
[14] B. Zhang, C. M. Ko, B. -A. Li and Z. -w. Lin, Phys. Rev. C **61**, 067901 (2000)
[15] Z. -W. Lin, C. M. Ko, B. -A. Li, B. Zhang and S. Pal, Phys. Rev. C **72**, 064901 (2005).
[16] S. Plumari, V. Baran, M. Di Toro, G. Ferini and V. Greco, Phys. Lett. B **689**, 18 (2010)
[17] G. 't Hooft, Phys. Rev. D **14**, 3432 (1976) [Erratum-ibid. D **18**, 2199 (1978)].
[18] M. Buballa, Phys. Rept. **407**, 205 (2005).
[19] Y. Nambu and G. Jona-Lasinio, Phys. Rev. **122**, 345 (1961); **124**, 246 (1961).
[20] T. Hatsuda and T. Kunihiro, Phys. Rept. **247**, 221 (1994).
[21] M. F. M. Lutz, S. Klimt and W. Weise, Nucl. Phys. A **542**, 521 (1992).
[22] M. Gyulassy and X. -N. Wang, Comput. Phys. Commun. **83**, 307 (1994).
[23] C. M. Ko, Q. Li and R. -C. Wang, Phys. Rev. Lett. **59**, 1084 (1987).
[24] C. -M. Ko and Q. Li, Phys. Rev. C **37**, 2270 (1988).
[25] A. Abada and J. Aichelin, Phys. Rev. Lett. **74**, 3130 (1995).
[26] V. Greco, V. Baran, M. Colonna, M. Di Toro, T. Gaitanos and H. H. Wolter, Phys. Lett. B **562**, 215 (2003).
[27] V. Greco, C. M. Ko and P. Levai, Phys. Rev. Lett. **90**, 202302 (2003); Phys. Rev. C **68**, 034904 (2003)
[28] V. Greco, C. M. Ko and R. Rapp, Phys. Lett. B **595**, 202 (2004).
[29] L. -W. Chen, C. M. Ko and B. -A. Li, Phys. Rev. C **68**, 017601 (2003); Nucl. Phys. A **729**, 809 (2003).
[30] J. Beringer *et al.* [Particle Data Group Collaboration], Phys. Rev. D **86**, 010001 (2012).